Nature Communications

https://doi.org/10.1038/s41467-025-68107-3

Article in Press

Breaking immiscibility barriers: ultrafast sintering of interlocked Cu-Fe-based composites

Received: 20 March 2025

Accepted: 16 December 2025

Cite this article as: Shen, S., Wu, Z., Liu, X. *et al.* Breaking immiscibility barriers: ultrafast sintering of interlocked Cu-Fe-based composites. *Nat Commun* (2025). https://doi.org/10.1038/s41467-025-68107-3

Shiji Shen, Zhenduo Wu, Xiaoye Liu, Si Lan & Chengwei Wang

Breaking Immiscibility Barriers: Ultrafast Sintering of Interlocked Cu-Fe-Based Composites

Shiji Shen[1,2,3]†, Zhenduo Wu[3]†, Xiaoye Liu[1,2], Si Lan[4]*, Chengwei Wang[1,2]*

[1]State Key Laboratory of Precision and Intelligent Chemistry, University of Science and Technology of China, Hefei, Anhui 230026, China

[2]Department of Materials Science and Engineering, University of Science and Technology of China, Hefei, Anhui, 230026, China

[3]City University of Hong Kong (Dongguan), Dongguan, Guangdong, 523000, China

[4]Herbert Gleiter Institute of Nanoscience, School of Materials Science and Engineering, Nanjing University of Science and Technology, Nanjing, Jiangsu, 210094, China

* Email: vcwang@ustc.edu.cn, lansi@njust.edu.cn,

†These authors contributed equally to this work.

Abstract

With increasingly stringent application environments, there is a growing demand for designing and fabricating of promising structural materials. Conventional metallurgical methods typically struggle to produce positive mixing enthalpy alloys with uniform microstructures and consistent properties due to mutual immiscibility and uncontrollable segregation during solidification. To this end, we employ a bottom-up approach to fabricate Cu-50 vol% $Fe_{55}Cr_{25}Mo_{16}B_2C_2$ positive mixing enthalpy composites, utilizing ultrafast high-temperature sintering and instantaneous quenching. The method effectively prevents liquid segregation during the molten state and allows precise control over the size and distribution of the two phases. In addition, incorporated metallic glass particles as the hard phase additives, which can quickly form the localized multi-phase nanocrystals and establish a robust interlocking structure with pure copper during rapid sintering. Upon rapid quenching, the two phases solidify with a tight and conformal interface, while the elemental cross-diffusion and phase separation are mitigated. The mechanical tensile strength of the resulting composite is approximately 8 times greater than that of pure Cu. The wear resistance improves by 40-50 times, and the Vickers hardness increases by a factor of 10. The innovative sintering method provides a feasible pathway for developing and manufacturing of positive mixing enthalpy composite materials.

Introduction

For thousands of years, traditional alloy design and development have primarily focused on systems with negative mixing enthalpy[1,2]. Expanding the compositional range of positive mixing enthalpy alloy systems and controlling the microstructural arrangement of different phases could lead to the development of materials with characteristics previously unseen in alloy materials, offering immense potential[3,4]. Unlike negative mixing enthalpy alloy systems, which can easily achieve highly uniform solid solution structures[5–7], positive mixing enthalpy systems face inherent challenges[8,9]. Due to the immiscibility of metals in the liquid phase and the prolonged heat treatment durations of conventional metallurgical methods, such as suction casting[10], vacuum hot pressing[11], high-pressure torsion[12], or mechanical repetitive rolling[13], the resulting positive mixing enthalpy systems tend to have severe phase separation and poor mechanical properties. Moreover, the temperature-dependent thermodynamic driving forces induce variations in elemental segregation kinetics, leading to uncontrolled heterogeneous microstructures of immiscible phases due to the instability of phase separation dynamics[14,15]. Despite decades of research, precisely controlling elemental segregation to achieve a uniformly distributed biphasic structure remains an unsolved challenge[16,17].

To address this issue, introducing intermediate elements has become a widely adopted strategy for inducing stable solid solutions[18,19]. For instance, adding a third component (e.g., Ni or Co) can reduce the overall mixing enthalpy or stabilize metastable phases, leading to greater elemental mixing and reduced segregation[20,21]. Nevertheless, the strategy necessitates precise regulation of alloying element stoichiometry and spatial distribution, concurrent maintenance of thermodynamic equilibrium, and interfacial stability across multiphase systems. Alternatively, multiscale

structural design and hierarchical heat treatment have also been employed in developing metals with positive mixing enthalpy[22]. Recent studies, however, have been limited to adding small amounts of positive mixing enthalpy elements (<0.5%) to either promote the precipitation of coherent nanophases (typically confined to phase diagram edges[5,6]) or form limited solid solutions[23,24]. While hypoeutectic doping leverages metastable phase diagrams to confine positive-enthalpy elements at grain boundaries, such compositional constraints inherently limit bulk-scale property engineering[25,26].

Given these constraints, we herein employ a bottom-up fabrication strategy for positive mixing enthalpy alloys, incorporating precise microstructure regulation to suppress high-temperature phase segregation. Based on the ultra-fast high-temperature sintering (UHS) technology[27,28], we have introduced an ultrafast cooling system to enable rapid quenching during the final stage of sintering, achieving ultra-high-temperature rapid sintering and quenching (UHSQ) **(Supplementary Figure 1a-b and Supplementary Movie 1)**. Combining ultra-high heating and quenching rates ensures a stable and controllable liquid-phase window in positive mixing enthalpy systems **(Figure 1a)**. This approach retains the high heating rate (500-1000 K /s) of the UHS process while providing an enhanced cooling rate (up to 1000 K /s at the sample surface; see **Figure 1b; Supplementary Figure 2 and Supplementary Movie 2)**. Specifically, the precursor compact was wrapped in zirconia (ZrO_2) fiber cloth for electrical insulation (**Supplementary Figure 1c)**, positioned between two carbon felts in an argon atmosphere, rapidly sintered for 10 seconds, and then immediately quenched in high thermal conductivity silicone oil at 243 K **(Figure 1c)**. Employing the UHSQ technique, we successfully sintered a Cu-50 vol% $Fe_{55}Cr_{25}Mo_{16}B_2C_2$ positive mixing enthalpy composites, denoted as Cu-Fe-based composite. Concurrent ultrafast

quenching (~1s) induces three critical microstructural evolutions: atomic-scale heterogeneity redistribution in metallic glass; dislocation substructure modification in copper; and nanoscale rivet-like interlocking at interfaces arising from differential thermal contraction coefficients. Due to differences in thermal shrinkage coefficient at the closely attached interface, a nanoscale interlocking rivet-like structure is formed, resulting in a highly robust interface **(Figure 1d)**. The sequential stages of UHSQ processing – including precursor assembly, Joule heating sintering and quenching – are visually documented in **Figure 1e and Supplementary Figure 3**. Metallic glasses demonstrate distinct thermal response across their glass transition temperature (T_g): Below T_g, they exhibit the rigidity of crystalline solids while retaining structural metastability; above T_g, viscous flow initiates until crystallization occurs, resulting in the restoration of rigidity[29]. This complex phase transition behavior enables effective coupling with positive enthalpy materials when sintering parameters (temperature/time) are precisely regulated. Crucially, at elevated temperatures above T_g, metallic glasses become supercooled liquid with increased fluidity that facilitate interfacial contact[30,31]. Implementing the paradigm, we fabricated Cu-Fe-based composites **(Figure 1f)** with submicron-scale elemental homogeneity, coarsening, and tightly attached phase interfaces. The resulting materials exhibit a yield strength of 684 MPa at room temperature, with a maximum Vickers hardness of 1297 HV and an average hardness of 931 HV. The yield strength was retained at approximately 290 MPa even at 923 K. This method successfully overcomes the limitations of previous techniques, enabling the fabrication of positive mixing enthalpy composite materials and significantly broadening the boundaries of composite metal synthesis.

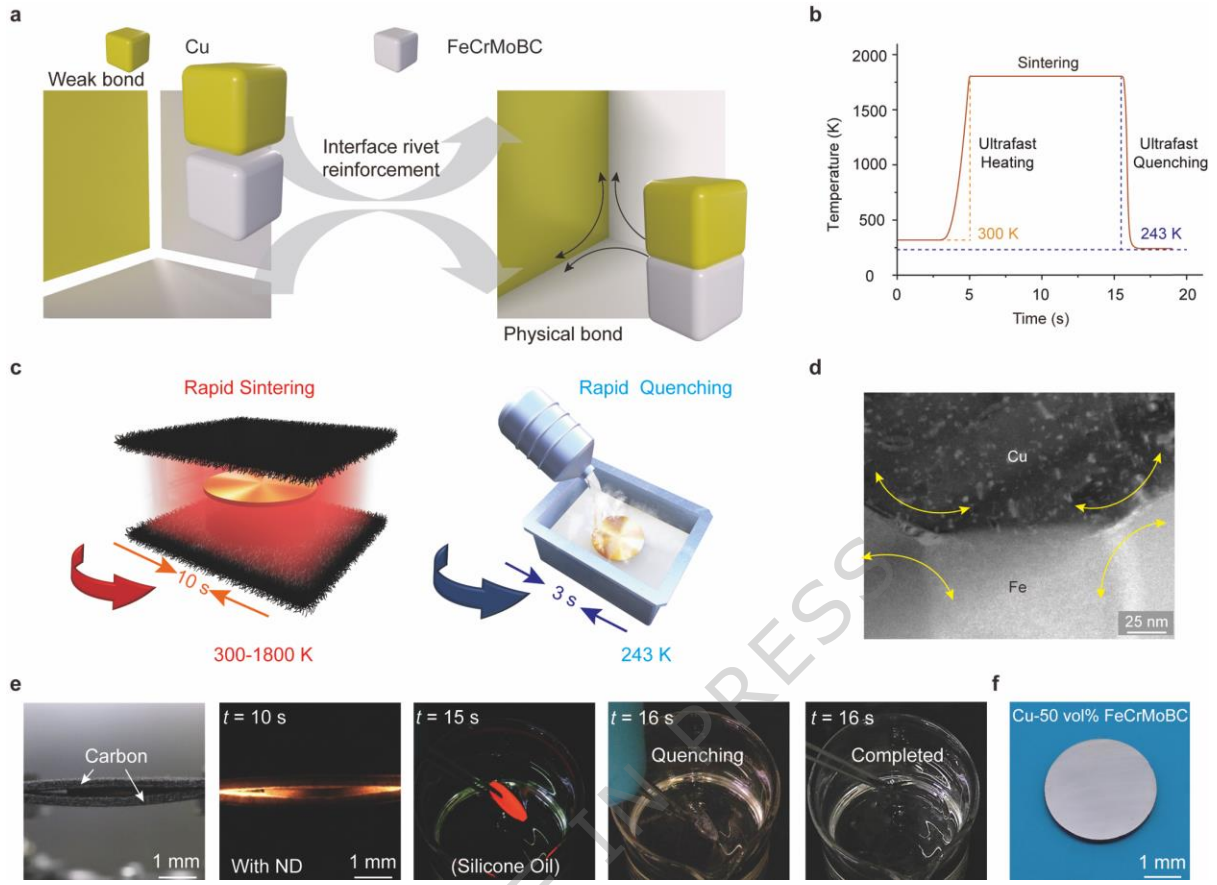

Figure 1. Schematic diagram of the UHSQ process for fabricating mechanically interlocked Cu-Fe-based composite. (a) Schematic illustration of the "interface riveting" mechanism. An initially weak contact between immiscible Cu and $Fe_{55}Cr_{25}Mo_{16}B_2C_2$ metallic glass particles is transformed into a strong, mechanically interlocked physical bond at the interface. (b) The schematic temperature-time profile of the UHSQ process, characterized by ultrafast heating (500~1000 K/s), a short sintering plateau at high temperature, and subsequent rapid quenching. (c) Schematic of the experimental procedure, showing the sample, housed in a ZrO_2 die, being rapidly heated between two carbon electrodes and then quickly submerged into a silicone oil bath for quenching. (d) Transmission electron microscope (TEM) images reveal rivet-like connections formed by physical deformation between Cu and FeCrMo nanocrystal. (e) A photographic

sequence capturing the key moments of the actual UHSQ process. (f) The Cu-Fe-based composite pellet with positive mixing enthalpy prepared by UHSQ sintering.

Results and Discussion

Fabrication and Microstructural Characterization of Cu-Fe-based Composites

The exceptional hardness of metallic glass is a significant advantage but the smooth surface poses challenges for interface attachment[32] **(Figure 2a and Supplementary Figure 4)**. Mechanical milling has been proven to be an effective method for enhancing the attachment between phases[33]. To verify this, we employed high-energy ball milling and observed notable changes in the covering degree between phases as a function of milling time **(Figure 2b-c and Supplementary Figure 5a)**. It was evident that $Fe_{55}Cr_{25}Mo_{16}B_2C_2$ metallic glass precursors subjected to high-energy ball milling exhibited significantly improved interfacial attachment with Cu particles. The continuous milling process not only introduces surface roughening into the $Fe_{55}Cr_{25}Mo_{16}B_2C_2$ metallic glass itself but also ensures uniform coverage of Cu on the surface of metallic glass particles[34], facilitating subsequent connection with the Cu phase during sintering **(Supplementary Figure 5b)**. Notably, the particle size of $Fe_{55}Cr_{25}Mo_{16}B_2C_2$ metallic glass remains unchanged during high-energy ball milling. Additionally, the starting $Fe_{55}Cr_{25}Mo_{16}B_2C_2$ metallic glass particles are generally large, highlighting a potential direction for future optimization by reducing the size of metallic glass particles **(Figure 2d)**.

To demonstrate the universality of our UHSQ technique, we fabricated Cu-$Fe_{55}Cr_{25}Mo_{16}B_2C_2$ composite materials with a 1:1 volume ratio, where the Fe content reached 27.5%, far exceeding that of conventional Cu-Fe alloys. As a comparison, we also employed various sintering techniques to prepare samples. The XRD patterns of samples prepared via UHS and traditional furnace

sintering were similar, displaying pure Cu phases **(Figure 2e left)**. Notably, in UHSQ specimens quenched within 1 second, weak crystalline peaks emerged **(Figure 2e right),** suggesting partial devitrification of the amorphous matrix. In contrast, specimens subjected to a 10-second dwell time prior to quenching achieved near-complete crystallization, restoring the equilibrium Fe-Cr-Mo phase assemblage.

Optical and scanning electron microscopy images **(Figure 2f)** demonstrate that conventional sintering (annealing at 1073 K for 2h in Ar_2, followed by annealing at 573 K for 6h) fails to mitigate elemental segregation in Cu-$Fe_{55}Cr_{25}Mo_{16}B_2C_2$ positive mixing enthalpy alloys, resulting in phase-separated Cu-rich and Fe-rich coarsened domains. This phenomenon primarily originates from thermocapillary-driven Marangoni convection during liquid-liquid phase separation, as described by the Cahn-Hilliard model[35,36]. In contrast, UHS leverages ultra-fast sintering rates to suppress elemental segregation and control the crystallization of the metallic glass reinforcements. Upon softening, the viscosity of the metallic glass temporarily behaves like an adhesive, tightly bonding the two phases and effectively extending the processing window. UHS is ultimately limited by the intrinsic immiscibility of positive enthalpy systems and subcritical cooling rates, permitting interfacial phase separation that generates porous weak interfaces **(Supplementary Figure 6a-c and Supplementary Figure 7)**. This interfacial failure is directly linked to the sintering duration; prolonging the high-temperature exposure allows for the severe phase segregation demonstrated in **Supplementary Figure 8d**. Minimizing the sintering time is therefore critical to kinetically trap the system and suppress elemental segregation (**Supplementary Figure 8a-c)**. Remarkably, UHSQ, with its ultrafast cooling rates, refines grain structures while retaining the advantages of UHS. Moreover, UHSQ precisely regulates the devitrification pathway of the amorphous matrix,

generating hierarchical microstructures that integrate nanocrystals with high-density lattice defects **(Figure 2f right and Supplementary Figure 6d)**. The extreme quenching rate triggers distinct nanoscale architectural interlocking through stress-induced transformation. The microscopic rivet-like architecture at the nanoscale firmly bonds the Cu–Fe interface while constraining the distribution of individual components, resulting in a homogeneous interlocked Cu-Fe-based composite structure **(Figure 3a, b)**.

The rapid quenching process induces the formation of a multiscale structure within the Fe-based metallic glass **(Supplementary Figure 9)**. Bright-field TEM imaging reveals a regular and uniform distribution of nanoscale crystal particles within the metallic glass **(Figure 3c)**. **Figure 3b** collectively demonstrates that the $Fe_{55}Cr_{25}Mo_{16}B_2C_2$ metallic glass devitrifies into a multi-phase nanocrystal, in which nanocrystalline Fe–Cr ferrite forms the continuous skeleton of the microstructure. The fcc Fe–Cr matrix surrounds and mechanically pins two secondary constituents, Mo-rich nanocrystals and Fe-rich areas. Bcc Mo-rich nanocrystals populate junctions and grain corners in a quasi-periodic manner, occupying ~14 vol % of the microstructure **(Supplementary Figure 10 and Supplementary Figure 11a-b)**, surrounding each Mo grain is a shell of bcc Fe ferrite. Notably, the Fe-rich areas contain a mixture of pure Fe, partially retained amorphous phase **(Supplementary Figure 11c, e)**, and ordered b2 intermetallic phases that contribute to the overall intricate structure **(Supplementary Figure 11d)**. The complex arrangement indicates an incomplete devitrification process, resulting in a multiphase nanocrystalline structure with retained amorphous pockets. The overall microstructure exhibits a high density of interfaces and structural complexity. This intricate structural architecture, arising from the controlled devitrification of the initial metallic glass, significantly influences the material's properties. These special nanocrystal

structural features are critical for coherent Cu-Fe interfaces with periodic misfit dislocations, which geometrically resemble traditional mortise-tenon interlocking structures. The interlocking of different rivet structures creates a tight interface, with a strong attachment between them (**Figure 3a**). Such microstructural control further contributes to the macroscopic uniformity of the composite. Furthermore, at different interface angles, no elemental cross-diffusion is observed, providing clear evidence that this technique effectively controls elemental segregation at the microscopic level **(Figure 3b right)**. Such unprecedented control over both structural hierarchy and elemental distribution redefines manufacturability limits for immiscible systems.

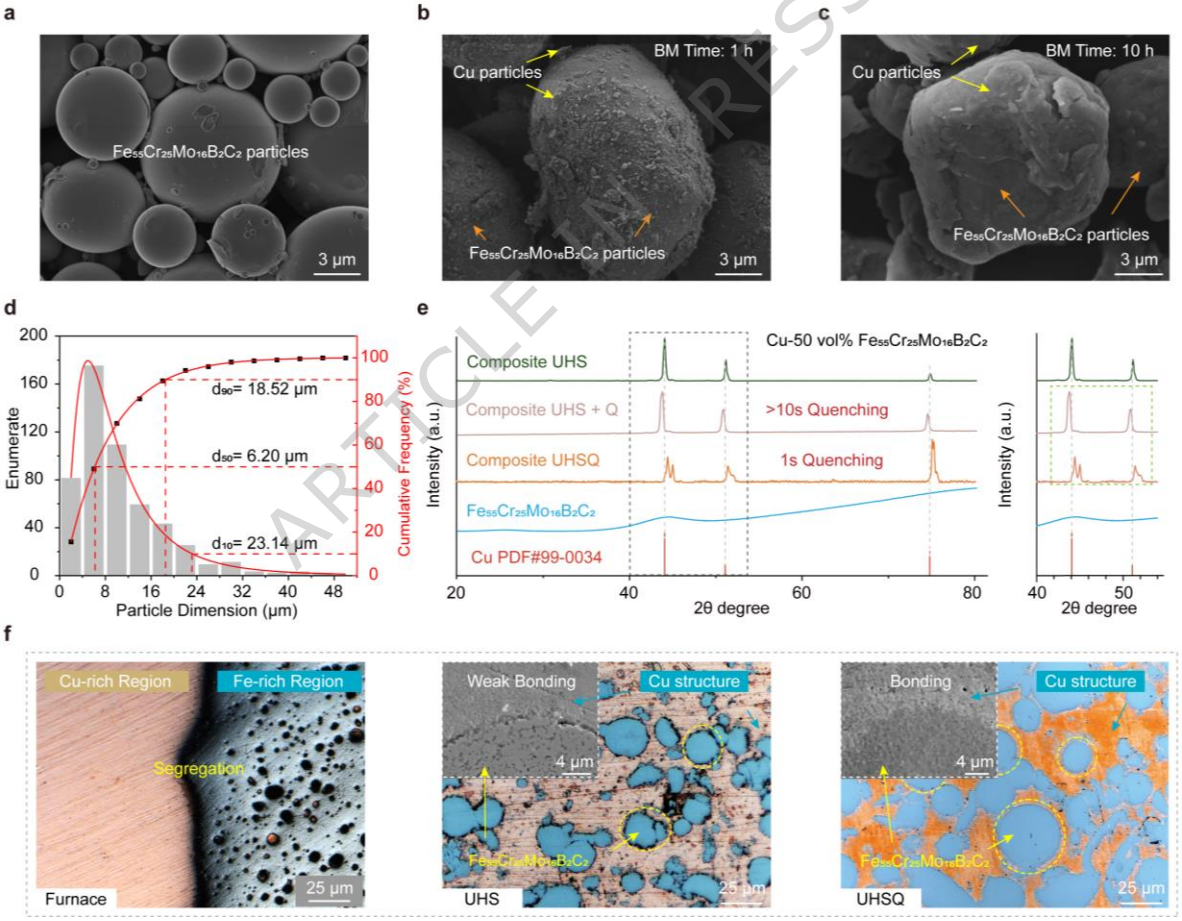

Figure 2. Sintering and Structural Characterization of Interlocked Cu-Fe-based Composite. (a) Representative SEM micrographs showing the morphology of $Fe_{55}Cr_{25}Mo_{16}B_2C_2$ metallic glass

particles. (b-c) The effect of high-energy ball milling for 1 h and 10 h, respectively, showing the progressive coating of the hard MG particles with ductile Cu to create an ideal precursor. (d) Statistical size distribution of ball-milled amorphous alloy particles. (e) XRD patterns and magnified regions of Cu-Fe-based composites fabricated via distinct sintering routes. (f) Optical micrograph of Cu-Fe-based composite processed by different sintering techniques. UHS and UHSQ methods suppress elemental segregation, with UHSQ further enabling a defect-free interfacial morphology.

Multi-scale Strengthening Mechanisms

We systematically compared the mechanical properties of materials processed under different sintering conditions. The optimized UHSQ-processed composites demonstrate a remarkable and comprehensive enhancement of mechanical properties, spanning bulk behavior (tensile and flexural strength) and surface performance (hardness and wear resistance). Using a composite with 50% $Fe_{55}Cr_{25}Mo_{16}B_2C_2$ as an example, the ultimate tensile yield strength reached approximately 685 MPa, which is 6.5 times higher than pure Cu **(Figure 3d)**. Remarkably, this strength advantage persists at elevated temperatures, with the composite maintaining 290 MPa yield strength at 923 K **(Figure 3e)**. For comparison, we prepared control samples **(Supplementary Figure 12)** with several key variations: reinforcement content, reinforcement type (pure Fe; Fe-based alloy), and high-temperature performance. All comparisons demonstrated significant improvements in mechanical performance originating from the unique, interlocking Cu-Fe interface where continuous Cu-rich and Fe-rich phases form interpenetrating networks resembling rivet joints, a structure forged by the UHSQ method. These results emphasize the substantial performance enhancement achieved by UHSQ-processed high-Fe-content positive mixing enthalpy composites,

including in high-temperature applications **(Supplementary Figure 13)**. The improvement is primarily attributed to the high strength of multi-phase nanocrystals[40].

SEM characterization reveals distinct morphological evolution between the samples prepared by UHS and UHSQ protocols **(Figure 3f-g)**. UHS-processed specimens exhibited compromised interfacial cohesion (average interfacial gap length: 2.1 ± 0.3 μm), accounting for their inferior mechanical performance **(Supplementary Figure 14)**. Suboptimal interfacial integrity is originated from prolonged thermal relaxation during UHS processing, where thermal expansion mismatch induced interfacial decohesion. In contrast, UHSQ samples displayed tight interfacial bonding. The main reason is that the ultra-fast cooling rate prevents the system from reaching equilibrium during the two-phase shrinkage process, enabling a strong attachment of different phases at high temperatures to be maintained at room temperature. The multi-phase nanocrystals formed strong interfaces with Cu, acting as rivets during tensile testing. The high interfacial bonding strength provided by the rivet-like structures is best demonstrated by the material's failure mechanism. Instead of debonding at the interface, failure occurs via brittle trans-particle fracture, where cracks propagate directly through the reinforcement phase itself **(Supplementary Figure 15)**. The behavior shows that the interface is stronger than the reinforcement material. The interfacial integrity is also reflected in the bulk mechanical properties shown in **Supplementary Figure 16.** While the difference in elastic modulus between the UHS and UHSQ samples contributes to the overall stress-strain response, the strength is predominantly attributed to a multiphase synergistic strengthening mechanism forged by the UHSQ process. The enhancement is not due to a change in intrinsic material stiffness but is a direct reflection of the strengthening effect from the improved interface bonding achieved by rapid quenching.

Fractography of UHSQ specimens revealed a homogeneous distribution of equiaxed dimples in the Cu matrix **(Figure 3g)**, indicative of good ductility. This structural uniformity is confirmed by Energy-dispersive X-ray spectroscopy (EDS) mapping of the same fracture regions, which shows no evidence of large-scale elemental segregation **(Supplementary Figure 17)**. The suppression of elemental diffusion is further corroborated at higher resolution by corresponding SEM and TEM-based EDS line scans performed on cross-sections **(Supplementary Figure 18)**. Overall, we believe the enhancement in mechanical strength of this structure is manifested at different levels. Macroscopically, the Cu-rich and Fe-rich phases form two distinct interwoven network structures, similar to a rivet configuration, imparting excellent strength and ductility to the sample. For the composite with a 1:1 volume ratio of Cu to $Fe_{55}Cr_{25}Mo_{16}B_2C_2$ metallic glass, the composite achieves 8.91% tensile ductility, while enhancing the material's overall strength and performance. Also, UHSQ allows for the adjustment of the Cu-Fe ratio to fine-tune the overall strength and ductility of the composite material. At the microscopic level, a small amount of $Fe_{55}Cr_{25}Mo_{16}B_2C_2$ metallic glass is dispersed within the Cu phase, creating a dispersion-strengthening effect that further improves mechanical performance **(Figure 3h)**. Furthermore, at the interface, the Cu-Fe phases bond seamlessly with no gaps, and the distribution of phases is uniform. Additionally, crystallization of the $Fe_{55}Cr_{25}Mo_{16}B_2C_2$ metallic glass leads to the formation of multi-phase nanocrystals, which exhibit remarkable strength to further enhance the material's overall performance. The synergistic combination of rivet-like reinforcement and dispersion strengthening offers a clear pathway for further performance optimization, which can be achieved by tailoring particle size and distribution. This multiscale design strategy, which combines macro-architectural

control with nanoscale precipitation engineering, provides a viable method for developing high-performance hybrid composites enhanced properties.

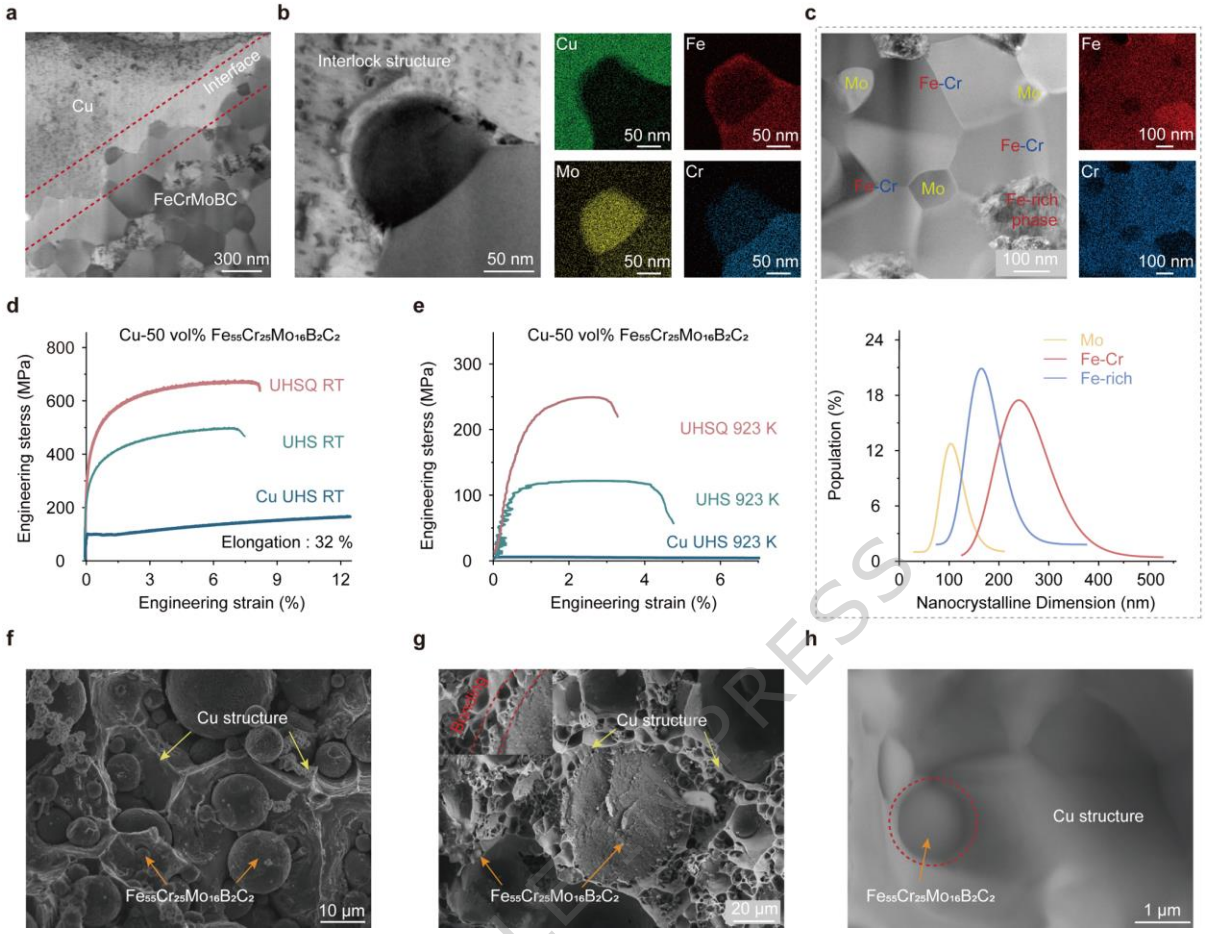

Figure 3. Multiscale microstructural and mechanical characterization of interlocked Cu-Fe-based Composite. (a) TEM image showing the clean, well-bonded interface between the Cu matrix and the Fe-based reinforcement. (b) Higher-magnification image of (a), revealing the nanoscale interlocking structure, with corresponding EDS maps showing the distinct phases. (c) HAADF-STEM analysis of the devitrified reinforcement, revealing a nano-architecture of an Fe-Cr matrix, Mo-rich precipitates, and Fe-rich phase, confirmed by EDS mapping. The plot below quantifies the size distribution of these nanocrystals. (d) Room-temperature tensile engineering stress-strain curves for the composites processed by UHS and UHSQ, compared with a monolithic Cu control sample. (e) Tensile engineering stress-strain curves at elevated-temperature (923 K) for the UHS and UHSQ-processed composites. (f-g) SEM images of the tensile fracture surface of

UHS and UHSQ-processed samples at room temperature. (h) SEM images showing the distribution of small metallic glass particles in the Cu matrix.

Hardness and Wear Behavior

As shown in **Figure 4a**, composites processed via UHSQ exhibit a significantly higher Vickers hardness than those prepared by UHS or pure Cu, achieving a high and consistent average hardness of 900 HV. The value is approximately 3 times higher than that of UHS-processed samples and 8 times higher than pure Cu **(Supplementary Figure 19)**. The hardness significantly exceeds the prediction from a simple linear rule of mixtures, indicating powerful synergistic strengthening effects. The origin of this synergy can be understood from the microhardness distribution shown in **Figure 4b**. The Fe-based reinforcement contains in-situ formed nanocrystalline intermetallic compounds and possesses a high intrinsic hardness of approximately 1100 HV, which provides a strong foundation for the composite's overall performance. Furthermore, the co-continuous, interlocking network architecture imposes a strong mechanical constraint on the softer Cu phase (which has a hardness of only ~90 HV). The constraint is enabled by a robust interface, which exhibits a high average hardness of ~500 HV and ensures efficient load transfer during indentation **(Supplementary Figure 20 and Supplementary Figure 21)**. Significant work hardening occurs in the ductile Cu matrix during deformation, further increasing its contribution to the overall hardness. It is the combination of these effects that results in the composite's hardness.

We summarized the hardness and electrical conductivity of Cu alloys, ceramic-metal composites, and metallic glasses reported in the literature[22,43-58] **(Figure 4c)**. The positive mixing enthalpy composites synthesized via UHSQ exhibit superior hardness compared to conventional Cu alloys, approaching the strength of metallic glasses and ceramic-metal composites. The electrical

conductivity ranges between 15-20% IACS, which is generally superior to metallic glasses, or ceramic-metal composites. This property holds significant potential in certain specialized materials, such as the conductive rails of electromagnetic launchers and the tracks of electromagnetic catapult systems, which require conductive materials that possess ultra-high hardness, heat resistance, and erosion resistance[41,42]. Moreover, the mechanical properties can be tuned by adjusting the content of $Fe_{55}Cr_{25}Mo_{16}B_2C_2$ metallic glass. Increasing the proportion improves strength, whereas decreasing it enhances ductility. This tunability highlights the potential for future optimization and broader applications.

We conducted wear tests on UHS and UHSQ-processed samples, which are compared to pure Cu. The tests applied a 10 MPa load, rotated at 500 r/min, with mass loss measured every 5 minutes. Fitted data curves show that UHSQ-processed composites demonstrate 40–50 times higher wear resistance than pure Cu **(Figure 4d)**. Samples with 25% and 50% $Fe_{55}Cr_{25}Mo_{16}B_2C_2$ metallic glass clearly exhibited strong Fe-based networks, contributing to greater macroscopic strength **(Figure 4e)**. Further SEM characterization of UHSQ-processed samples before and after 15 minutes and 60 minutes of wear testing revealed surface changes **(Figure 4f)**. The multi-phase nanocrystals showed minimal structural degradation, demonstrating their contribution to the enhancement of wear resistance. Strong interfaces and robust attachment also play a critical role in improving tribological performance. Photographic evidence of wear damage under identical test conditions highlights the superior wear resistance of UHSQ-processed composites compared to sintered pure Cu **(Supplementary Figure 22**). This study demonstrates an application view of positive mixing enthalpy composite materials. The seamless interlocking architecture with strong interfaces opens substantial possibilities for next-generation sliding electrical contacts, high-load tribological

components, and thermally stable conductor substrates. It addresses critical needs in sustainable energy systems, heavy machinery, and aerospace electronics, where concurrent electrical and mechanical robustness is essential.

Our method provides valuable guidance for designing advanced composite materials and highlights the potential of positive mixing enthalpy composites for structural and functional applications. The ability to tailor mechanical properties through compositional adjustments underscores the flexibility and scalability of this approach. In terms of scalability, the process's fast speed enables high-throughput manufacturing of large-area sheets and coatings, with current capabilities extending to near-centimeter thick bulk components; the primary focus for future scaling is addressing the engineering challenge of uniform quenching in even larger volumes. At its core, the method's success lies in the microscale rivet-like structure induced by rapid quenching, which produces an unprecedented strengthening effect at the interface. The approach produces homogeneous positive mixing enthalpy composites with a well-balanced structure, successfully controlling phase segregation while preserving both toughness and hardness. The universality of this approach suggests that leveraging its advantages in future material design will significantly expand the boundaries of composite material synthesis and development.

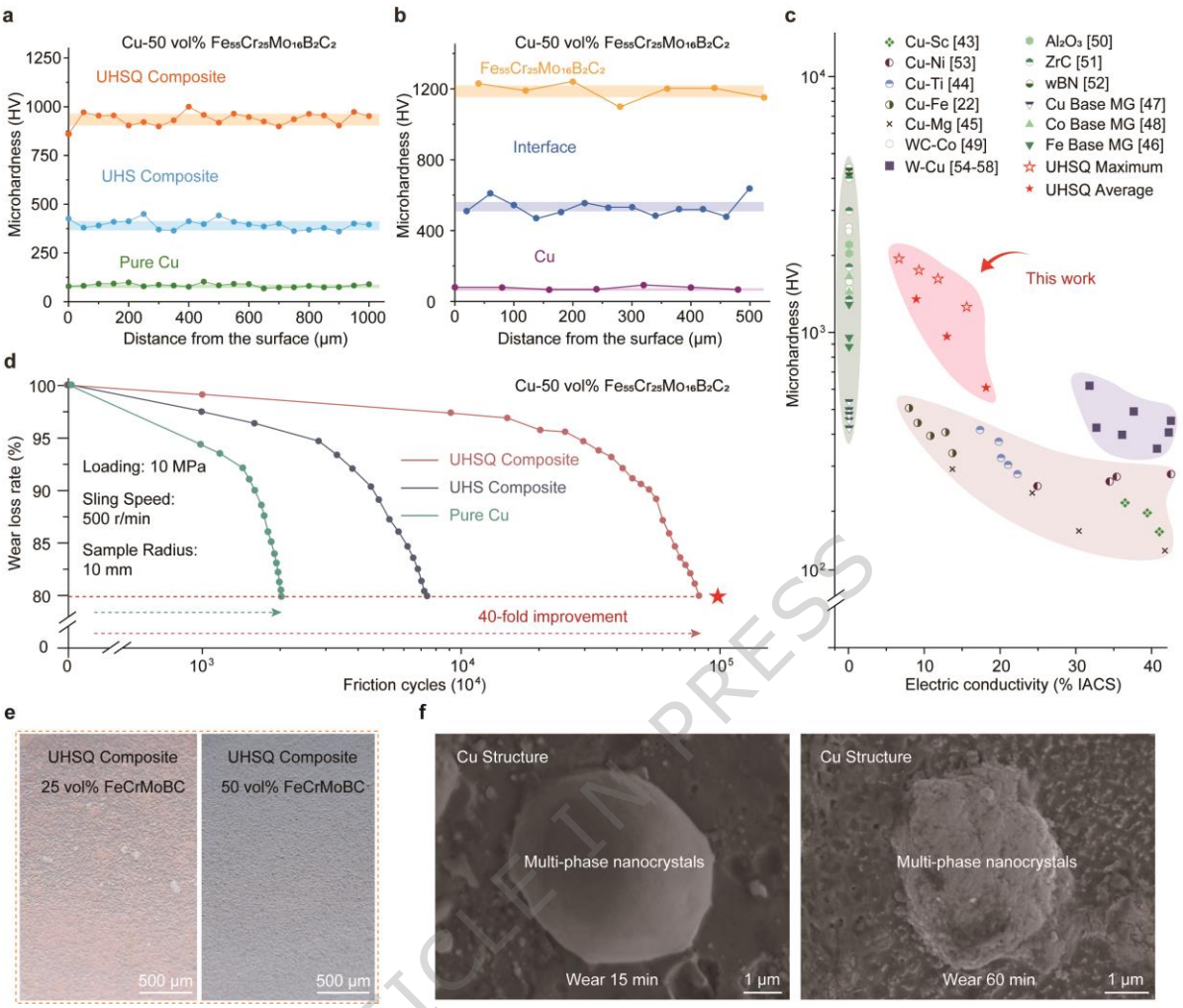

Figure 4. Mechanical and tribological properties of the Interlocked Cu-Fe-based Composite. (a) Microhardness profiles measured from the sample surface inwards for the UHSQ-processed composite, UHS-processed composite, and pure Cu. The shaded bands represent the standard deviation of the measurements. (b) Representative microhardness line scan across the Cu matrix, the Cu-Fe interface, and multi-phase nanocrystals. (c) The plot of microhardness versus electrical conductivity (% IACS), benchmarking the UHSQ-processed composite against various material classes reported in the literature[22,43-58]. (The colored background regions categorize different material systems: the pale pink region represents Cu-based alloys, the pale cyan region represents metallic glasses and ceramics, and the pale purple region corresponds to the W-Cu alloy family).

(d) Wear test results showing the wear loss rate as a function of friction cycles under a load of 10 MPa and a sliding speed of 500 r/min. (e) Optical micrographs of the worn surfaces of UHSQ-processed composites with 25 vol% and 50 vol% $Fe_{55}Cr_{25}Mo_{16}B_2C_2$ metallic glass, showing uniform wear tracks. (f) High-magnification SEM images tracking the morphology of multi-phase nanocrystals on the wear surface after 15 and 60 minutes of sliding.

We have developed a bottom-up approach using the ultra-high-temperature rapid sintering and quenching process to fabricate positive mixing enthalpy composites that uniquely combine the excellent ductility of pure Cu with ultra-high strength of hard alloys. The process leverages controlled partial crystallization during rapid heating to accelerate densification, while subsequent rapid quenching is then critical to preserve a key portion of the amorphous phase in the final microstructure. The strength of the composite originates from the robust, rivet-like interlocking interface forged between the Cu matrix and the multi-phase nanocrystals. Our interlocked Cu-Fe-based composite overcomes the traditional strength-ductility trade-off, achieving a good combination of electrical conductivity (15-20% IACS) and ultrahigh hardness (900 HV). This work demonstrates the tremendous potential of positive mixing enthalpy composites for advanced structural and functional applications. Our approach facilitates the development of previously inaccessible immiscible alloy systems. The good balance of properties makes the material highly promising for demanding applications, including advanced mechanical components, aerospace systems, and particularly for electromagnetic propulsion and high-performance tribological components. Ultimately, the UHSQ process preserves the unique properties of the constituent phases, significantly expanding the synthesis boundaries for advanced metallic composites.

Methods

Synthesis

The Cu-coated $Fe_{55}Cr_{25}Mo_{16}B_2C_2$ metallic glass precursor was prepared by mixing Cu (99%, Aladdin) and metallic glass (99% Yijinxc) in a 1:9 mass ratio using ZrO_2 as the grinding medium. High-energy ball milling was performed for 20 hours. The prepared coated precursor was then mixing with Cu (99%, Aladdin) in a 1:1 volume ratio. After further ball milling for 0.5 hours with ZrO_2 balls, the precursor was retrieved and shaped into a bulk form. Cold isostatic pressing at 250 MPa was employed to prepare a composite billet. Subsequently, the UHSQ technique was applied. The composite billet was wrapped in ZrO_2 fiber cloth, which serves as a high-temperature electrical insulator to prevent short-circuiting between the conductive sample and the carbon heaters. The high temperature of the carbon heater was monitored using a thermal infrared imager (628CH-L25).

Mechanical property characterization

The stress-strain curves at room temperature of the samples were measured with a Shimadzu AGS-X 10Kg tensile machine operated at a strain rate of $1 \times 10^{-3}\ s^{-1}$. An extensometer (RVX-112B) was used to ensure accurate strain reading. The stress-strain curves of the samples at high temperature were measured with an Instron 45582 tensile machine operated at a strain rate of $1 \times 10^{-3}\ s^{-1}$. Specific sample dimensions are provided in **Supplementary Figure 23b**. The hardness testing was performed using a Heng Yi MH-31 tester. The nanoindentation tests were performed on an Oxford Instruments Femto-Tools nano indenter and the specific test locations were selected based on the tensile fracture samples divided into regions at different distances (**Supplementary Figure 23a)**.

Materials characterization

The metallographic photographs wear taken after polishing and grinding using an optical microscope of ZEISS AXIO Imager (A1m), to observe the distribution of metallic glass and Cu. The scanning electron microscope (SEM) images were taken using a cold field emission scanning electron microscope (SU8220); Zeiss G500 SEM and Guoyi Quantum SEM5000X to observe the morphology of the sample. The crystal phases were examined by U1timaIV (Rigaku Corporation, Japan) XRD and scanned between 10° and 80° using Cu Kα radiation. A differential scanning calorimeter (DSC-Q200) from TA Instruments was used to monitor and measure the glass transition temperature (T_g) of the $Fe_{55}Cr_{25}Mo_{16}B_2C_2$ metallic glass. Furthermore, the detailed microstructures of the interfaces and the corresponding elemental distributions were analyzed using transmission electron microscopy (TEM) and energy-dispersive X-ray spectroscopy (EDS) on an FEI Talos F200X G2 system.

Data availability

Source data are provided with this paper. Additional experimental data which supports the findings of this study are available in the Supplementary Information and from the corresponding author upon request.

References:

1. Podgorsek, A., Jacquemin, J., Pádua, A. & Gomes, M. C. Mixing enthalpy for binary mixtures containing ionic liquids. *Chemical reviews* **116**, 6075–6106 (2016).
2. Zhang, W.-T. *et al.* Frontiers in high entropy alloys and high entropy functional materials. *Rare Metals* **43**, 4639–4776 (2024).
3. Jiang, S. *et al.* Ultrastrong steel via minimal lattice misfit and high-density nanoprecipitation. *Nature* **544**, 460–464 (2017).
4. Gao, J. *et al.* Facile route to bulk ultrafine-grain steels for high strength and ductility. *Nature* **590**, 262–267 (2021).
5. An, Z. *et al.* Negative mixing enthalpy solid solutions deliver high strength and ductility. *Nature* **625**, 697–702 (2024).
6. Cao, G. *et al.* Liquid metal for high-entropy alloy nanoparticles synthesis. *Nature* **619**, 73–77 (2023).
7. Li, X. Negative enthalpy raises strength and ductility. *Nature Materials* **23**, 178–178 (2024).
8. Hsu, W.-L., Tsai, C.-W., Yeh, A.-C. & Yeh, J.-W. Clarifying the four core effects of high-entropy materials. *Nature Reviews Chemistry* **8**, 471–485 (2024).
9. Sathiyamoorthi, P. & Kim, H. S. High-entropy alloys with heterogeneous microstructure: processing and mechanical properties. *Progress in Materials Science* **123**, 100709 (2022).
10. Chen, Z., Zhang, H. & Lei, Y. Secondary solidification behaviour of AA8006 alloy prepared by suction casting. *Journal of Materials Science & Technology* **27**, 769–775 (2011).
11. Tang, Y. *et al.* Overcoming strength-ductility tradeoff with high pressure thermal treatment. *Nature Communications* **15**, 3932 (2024).
12. Bachmaier, A., Kerber, M., Setman, D. & Pippan, R. The formation of supersaturated solid solutions in Fe–Cu alloys deformed by high-pressure torsion. *Acta Materialia* **60**, 860–871 (2012).
13. Kim, W. *et al.* Texture development and its effect on mechanical properties of an AZ61 Mg alloy fabricated by equal channel angular pressing. *Acta materialia* **51**, 3293–3307 (2003).
14. Schottelius, A. *et al.* Crystal growth rates in supercooled atomic liquid mixtures. *Nature Materials* **19**, 512–516 (2020).
15. Wang, C. P., Liu, X. J., Ohnuma, I., Kainuma, R. & Ishida, K. Formation of Immiscible Alloy Powders with Egg-Type Microstructure. *Science* **297**, 990–993 (2002).

16. He, J., Zhao, J. Z. & Ratke, L. Solidification microstructure and dynamics of metastable phase transformation in undercooled liquid Cu–Fe alloys. *Acta Materialia* **54**, 1749–1757 (2006).
17. Prokoshkina, D., Esin, V. A. & Divinski, S. V. Experimental evidence for anomalous grain boundary diffusion of Fe in Cu and Cu-Fe alloys. *Acta Materialia* **133**, 240–246 (2017).
18. Chen, K. X. *et al.* Morphological instability of iron-rich precipitates in CuFeCo alloys. *Acta Materialia* **163**, 55–67 (2019).
19. Moon, J. *et al.* A new strategy for designing immiscible medium-entropy alloys with excellent tensile properties. *Acta Materialia* **193**, 71–82 (2020).
20. Jiao, Z. B. *et al.* Synergistic effects of Cu and Ni on nanoscale precipitation and mechanical properties of high-strength steels. *Acta Materialia* **61**, 5996–6005 (2013).
21. Velthuis, S. G. E. te, Root, J. H., Sietsma, J., Rekveldt, M. Th. & Zwaag, S. van der. The ferrite and austenite lattice parameters of Fe–Co and Fe–Cu binary alloys as a function of temperature. *Acta Materialia* **46**, 5223–5228 (1998).
22. Wu, Y. *et al.* An overview of microstructure regulation treatment of Cu-Fe alloys to improve strength, conductivity, and electromagnetic shielding. *Journal of Alloys and Compounds* **1002**, 175425 (2024).
23. Zhou, B. C. *et al.* Mechanisms for suppressing discontinuous precipitation and improving mechanical properties of NiAl-strengthened steels through nanoscale Cu partitioning. *Acta Materialia* **205**, 116561 (2021).
24. Isheim, D., Gagliano, M. S., Fine, M. E. & Seidman, D. N. Interfacial segregation at Cu-rich precipitates in a high-strength low-carbon steel studied on a sub-nanometer scale. *Acta Materialia* **54**, 841–849 (2006).
25. Cai, P. *et al.* Local chemical fluctuation-tailored hierarchical heterostructure overcomes strength-ductility trade-off in high entropy alloys. *Journal of Materials Science & Technology* **214**, 74–86 (2025).
26. Xu, D., Wang, X. & Lu, Y. Heterogeneous-Structured Refractory High-Entropy Alloys: A Review of State-of-the-Art Developments and Trends. *Advanced Functional Materials* **34**, 2408941 (2024).
27. Wang, C. *et al.* A general method to synthesize and sinter bulk ceramics in seconds. *Science* **368**, 521–526 (2020).

28. Wang, C. *et al.* Rapid Synthesis and Sintering of Metals from Powders. *Advanced Science* **8**, 2004229 (2021).
29. Telford, M. The case for bulk metallic glass. *Materials today* **7**, 36–43 (2004).
30. Pan, J. *et al.* Extreme rejuvenation and softening in a bulk metallic glass. *Nature communications* **9**, 1–9 (2018).
31. Shimizu, F., Ogata, S. & Li, J. Yield point of metallic glass. *Acta materialia* **54**, 4293–4298 (2006).
32. Suryanarayana, C. & Inoue, A. Iron-based bulk metallic glasses. *International Materials Reviews* **58**, 131–166 (2013).
33. Wang, F. *et al.* Influence of two-step ball-milling condition on electrical and mechanical properties of TiC-dispersion-strengthened Cu alloys. *Materials & Design* **64**, 441–449 (2014).
34. Schroers, J. Processing of bulk metallic glass. *Advanced materials* **22**, 1566–1597 (2010).
35. Elliott, C. M. The Cahn-Hilliard model for the kinetics of phase separation. in *Mathematical models for phase change problems* 35–73 (Springer, 1989).
36. Saldi, Z. S. Marangoni driven free surface flows in liquid weld pools. *Delft University of Technology, The Netherlands* (2012).
37. Hossain, M. *et al.* Carbon stoichiometry and mechanical properties of high entropy carbides. *Acta Materialia* **215**, 117051 (2021).
38. Tsai, M.-H. & Yeh, J.-W. High-entropy alloys: a critical review. *Materials Research Letters* **2**, 107–123 (2014).
39. Ying, H. *et al.* Formation of strong and ductile FeNiCoCrB network-structured high-entropy alloys by fluxing. *Microstructures* **3**, 2023018 (2023).
40. Haubold, T., Bohn, R., Birringer, R. & Gleiter, H. Nanocrystalline intermetallic compounds—structure and mechanical properties. in *High Temperature Aluminides and Intermetallics* 679–683 (Elsevier, 1992).
41. Fair, H. Advances in electromagnetic launch science and technology and its applications. *IEEE Transactions on Magnetics* **45**, 225–230 (2009).
42. Weiming, Lu, J. & Liu, Y. Research progress of electromagnetic launch technology. *IEEE Transactions on Plasma Science* **47**, 2197–2205 (2019).

43. Dölling, J., Henle, R., Prahl, U., Zilly, A. & Nandi, G. Copper-Based Alloys with Optimized Hardness and High Conductivity: Research on Precipitation Hardening of Low-Alloyed Binary CuSc Alloys. *Metals* (2022) doi:10.3390/met12060902.
44. Fu, H. *et al.* Breaking hardness and electrical conductivity trade-off in Cu-Ti alloys through machine learning and Pareto front. *Materials Research Letters* **12**, 580–589 (2024).
45. Maki, K., Ito, Y., Matsunaga, H. & Mori, H. Solid-solution copper alloys with high strength and high electrical conductivity. *Scripta Materialia* **68**, 777–780 (2013).
46. Li, Y.-C., Zhang, C., Xing, W., Guo, S.-F. & Liu, L. Design of Fe-Based Bulk Metallic Glasses with Improved Wear Resistance. *ACS Applied Materials & Interfaces* **10**, 43144–43155 (2018).
47. Cheung, T. L. & Shek, C. H. Thermal and mechanical properties of Cu–Zr–Al bulk metallic glasses. *Journal of Alloys and Compounds* **434–435**, 71–74 (2007).
48. Zhang, G. *et al.* Preparation of non-magnetic and ductile Co-based bulk metallic glasses with high GFA and hardness. *Intermetallics* **107**, 47–52 (2019).
49. He, J. & Schoenung, J. M. A review on nanostructured WC–Co coatings. *Surface and Coatings Technology* **157**, 72–79 (2002).
50. Krell, A. High-temperature hardness of Al2O3-base ceramics. *Acta Metallurgica* **34**, 1315–1319 (1986).
51. Balko, J. *et al.* Nanoindentation and tribology of VC, NbC and ZrC refractory carbides. *Journal of the European Ceramic Society* **37**, 4371–4377 (2017).
52. Liu, Y. *et al.* Hardness of Polycrystalline Wurtzite Boron Nitride (wBN) Compacts. *Scientific Reports* **9**, 10215 (2019).
53. Ban, Y. *et al.* Properties and precipitates of the high strength and electrical conductivity Cu-Ni-Co-Si-Cr alloy. *Journal of Materials Science & Technology* **93**, 1–6 (2021).
54. Han, T. et al. W–Cu composites with excellent comprehensive properties. C*omposites Part B: Engineering* **233**, 109664 (2022).
55. Duan, Q. et al. Synergistic Enhancement of Mechanical Properties and Electrical Conductivity of Immiscible Bimetal: A Case Study on W–Cu. *Engineering* **46**, 224–235 (2025).

56. Liu, J.-K., Wang, K.-F., Chou, K.-C. & Zhang, G.-H. Fabrication of ultrafine W-Cu composite powders and its sintering behavior. *Journal of Materials Research and Technology* **9**, 2154–2163 (2020).
57. Hou, C., Cao, L., Li, Y., Tang, F. & Song, X. Hierarchical nanostructured W-Cu composite with outstanding hardness and wear resistance. *Nanotechnology* **31**, 084003 (2020).
58. Xiaoyong, Z., Jun, Z., Junling, C. & Yucheng, W. Structure and Properties of W-Cu/AlN Composites Prepared via a Hot Press-Sintering Method. *Rare Metal Materials and Engineering* **44**, 2661–2664 (2015).

Acknowledgements

This work was supported by the National Natural Science Foundation of China (Grant Nos. 52272249 to C.W., 52201190 to Z. Wu., 22209165 to C.W. and 52222104 to S.L.). Z. Wu acknowledges the financial support from the Department of Science and Technology of Guangdong Province (No. 2024TQ08C536), the Guangdong and Hong Kong Universities '1+1+1' Joint Research Collaboration Scheme, and Guangdong Basic and Applied Basic Research Foundation (No. 2024A1515010964).

We sincerely thank Professor Laima Luo from Hefei University of Technology for her support with testing and thank Sheng Peng, Shangshu Wu and Xiao Dong from City University of Hong Kong (Dongguan) for their valuable assistance.

We thank Shengquan Fu at Instruments Center for Physical Science, University of Science and Technology of China for assistance with the OXFORD Femto-Tools Nano Indenter (installed on CIQTEK Co., Ltd., FESEM5000X) measurements and characterizations. We also thank Dr. Jie Tian from the Material Test and Analysis Lab, Engineering and Materials Science Experiment Center at the University of Science and Technology of China, and Jianliu Huang from Carl Zeiss China for their valuable discussions and technical support with the Zeiss G500 SEM. The TEM work was partially carried out from Scientific Compass (www.shiyanjia. com).

Author contributions

C.W., Z.W., and S.S. conceived and designed the UHSQ experiments. S.S. conducted the UHSQ sintering experiments, metallographic analysis, mechanical property testing, TEM imaging, and SEM imaging with EDS mapping. S.S. also prepared the samples, performed XRD measurements, and carried out XRD characterization. C.W., S.L., Z.W., X.L., and S.S. wrote and revised the

manuscript. All authors contributed to the discussion of results and provided comments on the manuscript.

Competing interests

The authors declare no competing interests.

Editor's Summary

Immiscibility limits the performance of positive mixing enthalpy alloys. Here, the authors apply ultrafast sintering and quenching to fabricate mechanically interlocked Cu-Fe composites with good strength and conductivity.

Peer review information: *Nature Communications* thanks the anonymous reviewers for their contribution to the peer review of this work. A peer review file is available.